

Bayesian Modeling for Exposure Response Curve via Gaussian Processes: Causal Effects of Exposure to Air Pollution on Health Outcomes

Boyue Ren¹, Xiao Wu², Danielle Braun^{2,3}, Natesh Pillai⁴, and Francesca Dominici^{2,*}

¹Psychiatric Biostatistics Laboratory, McLean Hospital

²Department of Biostatistics, Harvard T.H. Chan School of Public Health

³Department of Data Sciences, Dana Farber Cancer Institute

⁴Department of Statistics, Harvard University

Abstract

Motivated by environmental health research on air pollution, we address the challenge of estimation and uncertainty quantification of causal exposure-response function (CERF). The CERF describes the relationship between a continuously varying exposure (or treatment) and its causal effect on a outcome. We propose a new Bayesian approach that relies on a Gaussian process (GP) model to estimate the CERF. We parametrize the covariance (kernel) function of the GP to mimic matching via a Generalized Propensity Score (GPS). The tuning parameters of the matching function are chosen to optimize covariate balance. Our approach achieves automatic uncertainty evaluation of the CERF with high computational efficiency, enables change point detection through inference on derivatives of the CERF, and yields the desired separation of design and analysis phases for causal estimation. We provide theoretical results showing the correspondence between our Bayesian GP framework and traditional approaches in causal inference for estimating causal effects of a continuous exposure. We apply the methods

to 520,711 ZIP-code-level observations to estimate the causal effect of long-term exposures to $\text{PM}_{2.5}$ on all-cause mortality among Medicare enrollees in the United States.

1 Introduction

A critically important scientific question in social, economic, and health sciences is whether there is a causal relationship between a continuously varying exposure (or a treatment) and an outcome. In particular in environmental health, we are interested in estimating the shape of a causal exposure response function (CERF) representing the relationship between long-term exposure to air pollution (such as fine particulate matter, $\text{PM}_{2.5}$, or other criteria pollutants) and a health outcome (e.g., the risk of hospitalization or death). The Environmental Protection Agency (EPA) in the US relies on the shape of the estimated exposure response function (ERF) from epidemiological studies to decide whether or not to lower the National Ambient Air Quality Standards (NAAQS). Evidence of increased health risks at exposure levels below the NAAQS suggests the NAAQS should be revised (EPA, 2019; Di et al., 2017a,b).

Recently, the decision as whether or not to lower the NAAQS for $\text{PM}_{2.5}$ has been even more controversial than in the past. Some scientists have argued that epidemiological studies that estimate the ERF via regression approaches do not provide evidence of causality and therefore should be dismissed when making air pollution regulatory decisions (Chartered Clean Air Scientific Advisory Committee, 2018; Goldman and Dominici, 2019). Dominici and Zigler (2017) argued that there are at least three notions of what constitutes evidence of causality in air pollution epidemiology, which are equally important. The first is causality inferred from evidence of biological plausibility. The second is consistency of results across many epidemiological studies and adherence to Bradford Hill causal criteria (Hill, 1965). The third is the use of causal inference methods. Under certain assumptions, causal inference methods are more robust to model misspecification compared to traditional regression approach. In addition, many causal inference methods explicitly enforce covariate balance to address potential confounding, making them the ideal analytic approaches to isolate causal relationships.

The majority of causal inference methods make the simplifying assumption of a binary exposure (or treatment) (Rosenbaum and Rubin, 1983; Rubin and Thomas, 1996; Hernán et al., 2000; Robins, 2000; Bang and Robins, 2005; Van der Laan and Rose, 2011). Early developments on CERF estimation (Hirano and Imbens, 2004; Robins, 2000; Robins et al., 1994) focus on weighting approaches and rely on the extended propensity score—Generalized Propensity Score (GPS)—for continuous treatment. These approaches are sensitive to misspecification of the GPS model. Doubly-robust approaches (Kennedy et al., 2017; Colangelo and Lee, 2020) that resolve the reliance on correctly specified GPS models in weighting approaches are proposed recently and some of them utilize weighting functions that explicitly satisfy covariate balancing condition (Schulz and Moodie, 2020). Alternative causal inference approaches, which by design optimize covariate balance (Zubizarreta, 2012; Zubizarreta et al., 2014; Zubizarreta, 2015; Wang and Zubizarreta, 2019), have been developed mostly for binary exposures. Extensions of this framework to the continuous exposure setting (Kallus and Santacatterina, 2019; Vegetabile et al., 2021) are proposed by defining a balancing metric (e.g., entropy) that is compatible with continuous exposures. Approaches based on matching for CERF estimation that are robust against misspecification of the GPS and outcome models are scarce in literature. Wu et al. (2018, 2020) introduced a GPS caliper matching framework to increase robustness and interpretability in both the design and analysis stages, with the ability to assess explicitly covariate balance of the pseudo-population implied by matching.

Although the literature on CERF is rich and rapidly evolving, there are two major unresolved challenges that are enormous bottlenecks. First, because most of these approaches are developed under the frequentist paradigm, assessing the uncertainty can become computationally intensive as it often relies on resampling methods such as bootstrap (Wu et al., 2018). Second, in environmental epidemiology in the context of $\text{PM}_{2.5}$ exposure, the central question is to assess as whether there is a low exposure level beyond which there is no evidence of an adverse causal effect on health (i.e. safe level) (Pope III et al., 2015). This question can be addressed by identifying change points of the CERF, which can be accomplished by estimating the derivatives of the CERF (Berhane and Molitor, 2008). To our knowledge, existing methods (in the context of regression or causal inference) do not provide a straightforward approach for quantifying the evidence of derivatives of CERF. Even

if the estimates of derivatives can be constructed, the uncertainty of these estimates would involve heavy computation, rendering inference on derivatives inaccessible and in turn hindering efficient detection of change points.

In this paper we introduce a Gaussian process (GP) approach for nonparametric modeling and estimation of CERF of air pollutants on all-cause mortality. GPs (Rasmussen, 2006) can be viewed as distributions over real-valued functions and therefore they offer a Bayesian nonparametric framework for inference of highly nonlinear latent functions from observed data. To estimate an ERF that has a causal interpretation, we introduce a novel parameterization of the covariance (kernel) function of the GP that is purposely specified to exactly match units via the GPS. To maintain the desirable property of separation of the design and analysis phase on causal inference approaches (Rubin et al., 2008), we introduce a tuning approach for the unknown hyper-parameters of the GP by optimizing a GP-induced covariate-balance metric. We show via theoretical arguments that our proposed approach is equivalent to an exact matching algorithm proposed by Wu et al. (2018). Our method overcomes the aforementioned challenges that are present in the previously proposed methods for estimation of CERFs via 1) a non-parametric outcome model for flexible estimation of CERFs; 2) introducing a Bayesian framework for the estimation of CERFs with automatic uncertainty evaluation through posterior inference; 3) straightforward estimation of derivatives of CERFs as well as its uncertainty, which in turn promotes reliable inference regarding potential change-points. In addition, we also note the computational challenges that are inherent to a GP-based approach when the sample size is large (our data application involves more than 0.5 million observations), which is not uncommon in large scale environmental health research. To improve computational scalability we apply a nearest-neighbor (nnGP) approximation (Datta et al., 2016) of GPs to facilitate scalability of the proposed method.

Via a simulation study, we verify that the proposed GP model can accurately recover the population average CERF from observational studies. We also compare the performance of our method to several competitors for estimating the CERF under a variety of settings and confirm the GP model achieves high accuracy in most settings. Our methodology and models are motivated by a dataset that includes a nationally representative sample of 68.5 million Medicare enrollees with

around 570 million person years, which are aggregated into 520,711 ZIP-code-level observations. We use this dataset to estimate the causal effect of $\text{PM}_{2.5}$ on all-cause mortality.

2 Medicare dataset

The details of the dataset are described in Wu et al. (2020). Briefly, we have assembled a longitudinal cohort of over 68.5 million Medicare (elderly) enrollees for the period 2000-2016. Within the Medicare cohort a unique patient ID is assigned to each enrollee to allow tracking over time, including date of death. We have relied on highly spatio-temporally (daily and at $1 \text{ km} \times 1 \text{ km}$ grids) resolved ambient $\text{PM}_{2.5}$, NO_2 , and ozone concentrations, estimated and validated from previously published prediction models (Di et al., 2019a,b; Requia et al., 2020). The place of residence of each Medicare enrollee is only available at the ZIP-code-level; therefore, we have used zonal statistics to aggregate air pollution predictions from $1 \text{ km} \times 1 \text{ km}$ grids to ZIP-codes by year. For each ZIP-code, we have computed the annual averages of $\text{PM}_{2.5}$ and NO_2 concentrations and warm-season (April 1st through September 30th) average for ozone. In Figure 1 left panel, we visualize the ZIP-code-level average concentrations of $\text{PM}_{2.5}$ from 2000 to 2016 in the US. We find that $\text{PM}_{2.5}$ tends to be higher in the Eastern US.

Information on neighborhood socioeconomic status (SES) factors and demographics is available from the US Census Bureau at the ZIP-code-level. We derive 12 variables from these SES factors and demographics, including average BMI, percent of smokers, race composition, median household income and house value, percent population and households below poverty level, distribution of educational attainment (college, some college, high school, not completed high school), population density, sex composition, percent of owner occupied housing and census region. In addition, we have information on annual average temperature and humidity in summer and winter, percent of dual eligibility (Medicare and Medicaid) and average age at enrollment. We obtain a total of 520,711 ZIP-code-level observations of these 18 factors and concentrations of $\text{PM}_{2.5}$, ozone and NO_2 from 2000 to 2016. Individual-level information for enrollees, including sex and age, are available through Medicare files. We aim to estimate the causal effects of $\text{PM}_{2.5}$ on all-cause mortality, while

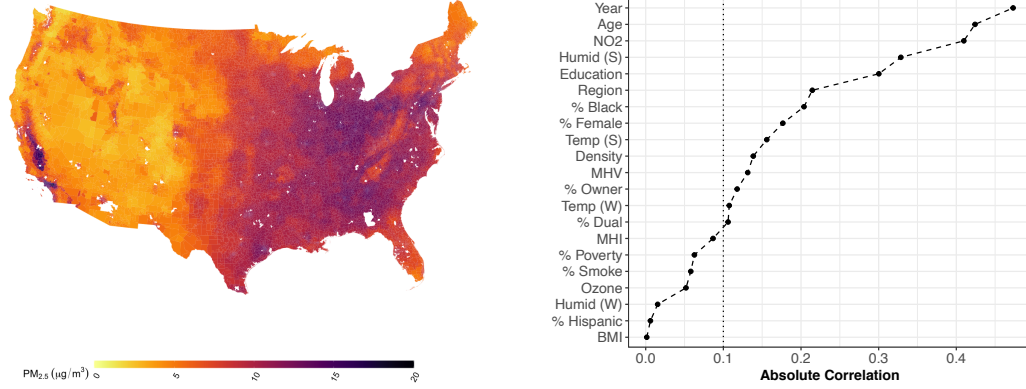


Figure 1: **(Left)** ZIP-code-level average concentrations of $PM_{2.5}$ from 2000 to 2016. Areas in white are those without $PM_{2.5}$ measurements. **(Right)** Correlations between $PM_{2.5}$ and other variables. Age = average age at enrollment; Education = proportion of below high school education; Humid (S) and (W) = average summer and winter humidity; Region = census region; Temp (S) and (W) = average summer and winter temperature; Density = population density; % Owner = % owner-occupied housing; % Dual = proportion of dual eligibility of Medicare and Medicaid; MHI = median home value; MHI = median household income; BMI = average BMI.

controlling for potential confounding effects.

In Figure 1 right panel, we illustrate the correlations between $PM_{2.5}$ and the other two pollutants as well as year and all 18 ZIP-code-level factors. We calculate these correlations using all ZIP-code-by-year observations and assume that these observations are independent. Most of the correlations are higher than 0.1. This motivates the need to adjust for these variables when estimating CERF of $PM_{2.5}$.

We quantify the burden of all-cause mortality using ZIP-code-level annual mortality rates. To estimate the mortality rate, we aggregate original age-at-death Medicare data into year-by-ZIP-code count data, which is defined as the number of deaths and the associated person-year for a ZIP-code in a certain year. We further stratify this data by enrollees' sex (male or female) and age at enrollment (younger than 75 or not) to control for confounding effects associated with individual-level variables. Specifically, we denote by $d_{i,g,t}$ the total number of deaths in stratum g in ZIP-code i and year $t \in \{2000, 2001, \dots, 2016\}$. We denote by $D_{i,g,t}$ the corresponding total person-year. The four stratum-specific datasets contain different numbers of ZIP-code-by-year observations with non-

zero $D_{i,g,t}$ (Table 1). We only use two categories for age and race to make sure that the number of observations in each resulting stratum with non-zero $D_{i,g,t}$ is large enough. The estimated mortality rate at year t , ZIP-code i and stratum g is then $\hat{\lambda}_{i,t,g} = d_{i,g,t}/D_{i,g,t}$. We also consider an age-sex-adjusted overall mortality rate $\hat{\lambda}_{i,t} = \sum_{g \in G_{i,t}} \lambda_{i,t,g}/|G_{i,t}|$ in ZIP-code i and year t , where $G_{i,t}$ is the set of strata where $D_{i,g,t} \neq 0$ and $|G_{i,t}|$ is the cardinality of $G_{i,t}$.

Table 1: Number of ZIP-code-by-year observations in each stratum

< 75 Years old		≥ 75 Years old	
Male	Female	Male	Female
516,060	515,108	477,028	496,378

3 GP models for CERF

Let $y_i \in \mathbb{R}$ be the outcome, $w_i \in \mathbb{R}$ be the exposure level, and $c_i \in \mathbb{R}^p$ be the vector of observed covariates for subject i , and let $\mathcal{S} = \{(y_i, w_i, c_i); i = 1, \dots, N\}$ be the observed data. The random variable $Y_i(w)$ denotes the potential outcome for subject i when he/she is exposed to a level w of a given exposure. Throughout the manuscript, we use capital letters to denote random variables and lower case letters for observed values of these random variables. As in Hirano and Imbens (2004), we define the GPS for subject i as $s_i = s(w_i, c_i) = p(w_i|c_i)$. Under the assumption of consistency (see below), $Y_i(w_i)$ is observed and equal to y_i . Note that $Y_i(w)$ is missing for $\forall w \neq w_i$. The population average causal exposure-response function (CERF) is denoted by $R(w)$ and is defined as $R(w) = \mathbb{E}(Y_i(w))$. To estimate $R(w)$, we first consider the estimation of $Y_i(w)$ for every subject i . In this section we first introduce the key assumptions that will allow us to identify the potential outcomes $\{Y_i(w) \forall w \neq w_i\}$ from the observed data \mathcal{S} .

Assumption 1. (Strong unconfoundedness) For any $n \in \mathbb{N}^+$, and $w_1, \dots, w_n \in \mathcal{W} = [w^0, w^1]$, the joint distribution of potential outcomes of subject i , $(Y_i(w_1), \dots, Y_i(w_n))$ is independent of the received exposure level W_i , conditional on the covariates vector C_i .

Assumption 2. (Consistency) The observed outcome y_i for subject i which has exposure level w_i is equal to the potential outcome $Y_i(w_i)$.

Assumption 3. (Overlap) For all values of c_i , the conditional density $p(w_i|C_i = c_i) > 0$ for any $w_i \in \mathcal{W} = [w^0, w^1]$.

Assumption 4. (Smoothness) The counterfactual outcome $Y_i(w, s_i)$ is continuous with respect to both exposure w and GPS s_i .

Under the strong unconfoundedness assumption, we can factorize the joint distribution $p(Y_i(w), W_i, C_i)$ as $p(Y_i(w)|C_i) \times p(W_i, C_i)$. We assume a GP model (Rasmussen, 2006) for $p(Y_i(w)|C_i)$:

$$\begin{aligned} Y_i(w) &= f(w, c_i) + \epsilon_i, \\ f(w, c) &\sim GP(\mu(w, c), k((w, c), (w', c'))), \end{aligned} \tag{1}$$

where $\epsilon_i \sim N(0, \sigma^2)$ is a noise term. $\mu(\cdot)$ and $k(\cdot, \cdot)$ are the mean and covariance function of the GP. For the rest of this section we assume that all the hyper-parameters, including σ^2 and the hyperparameters in $\mu(\cdot)$ and $k(\cdot, \cdot)$, are known and fixed. In Section 3.2, we will relax this assumption. We model and estimate the GPS $p(w|c)$ using machine learning approaches, such as gradient boosting (Chen and Guestrin, 2016), to reduce potential misspecification of the GPS model. As detailed in Section 3.1, the estimated GPS will be incorporated into the specification of the covariance function k . Please note that all our analyses will be conditional on the observed set of covariates and therefore we will not specify a model for $p(C)$.

Let $\mathbf{Y} = (Y_i(w_i); i = 1, \dots, N)^\top$, $\mathbf{m} = (\mu(w_i, c_i); i = 1, \dots, N)^\top$, $\boldsymbol{\kappa}_i(w) = (k((w, c_i), (w_j, c_j)); j = 1, \dots, N)^\top$ and $\mathbf{K} = (k((w_i, c_i), (w_j, c_j)); i, j = 1, \dots, N)$. Based on the GP model, we have

$$\begin{bmatrix} Y_i(w) \\ \mathbf{Y} \end{bmatrix} \sim MVN \left[\begin{pmatrix} \mu(w, c_i) \\ \mathbf{m} \end{pmatrix}, \begin{pmatrix} k((w, c_i), (w, c_i)) & \boldsymbol{\kappa}_i^\top(w) \\ \boldsymbol{\kappa}_i(w) & \mathbf{K} \end{pmatrix} + \sigma^2 I_{N+1} \right],$$

where I_{N+1} is the $(N+1)$ -dimensional identity matrix. The posterior distribution $Y_i(w)|\mathbf{Y}$ follows a normal distribution $N(m_i(w), \sigma_i^2(w))$, where

$$\begin{aligned} m_i(w) &= \mu(w, c_i) + \boldsymbol{\kappa}_i^\top(w) (\mathbf{K} + \sigma^2 I_N)^{-1} (\mathbf{Y} - \mathbf{m}) \\ \sigma_i^2(w) &= k((w, c_i), (w, c_i)) + \sigma^2 - \boldsymbol{\kappa}_i^\top(w) (\mathbf{K} + \sigma^2 I_N)^{-1} \boldsymbol{\kappa}_i(w). \end{aligned}$$

Under the assumption of consistency, we have $\mathbf{Y} = \mathbf{y} = (y_1, \dots, y_N)$. Therefore we can estimate $Y_i(w)$ by:

$$\hat{Y}_i(w) = \mu(w, c_i) + \boldsymbol{\kappa}_i^\top(w) (\mathbf{K} + \sigma^2 I_N)^{-1} (\mathbf{y} - \mathbf{m}). \quad (2)$$

The corresponding estimate of $R(w)$ is $\hat{R}(w) = N^{-1} \sum_{i=1}^N \hat{Y}_i(w)$. To quantify the statistical uncertainty of $\hat{R}(w)$, we first note that the conditional covariance matrix $\boldsymbol{\Sigma}(w)$ of $\hat{\mathbf{Y}}(w) = (\hat{Y}_1(w), \dots, \hat{Y}_N(w))$ given \mathcal{S} is

$$\boldsymbol{\Sigma}(w) = \mathbf{K}(w) + \sigma^2 I_N - \tilde{\mathbf{K}}(w)^\top (\mathbf{K} + \sigma^2 I_N)^{-1} \tilde{\mathbf{K}}(w),$$

where $\mathbf{K}(w) = [k((w, c_i), (w, c_j)); i, j = 1, \dots, N]$ and $\tilde{\mathbf{K}}(w) = [k((w, c_i), (w_j, c_j)); i, j = 1, \dots, N]$.

We evaluate the statistical uncertainty of $\hat{R}(w)$ using the posterior variance $\sigma_R^2(w) = N^{-2} \mathbf{1}_N^\top \boldsymbol{\Sigma}(w) \mathbf{1}_N$, where $\mathbf{1}_N$ is the all-one vector of length N .

When the hyper-parameters are unknown, we need to first select their values for the estimation of $Y_i(w)$. Typically, this can be achieved via fully Bayesian inference by putting hyper-priors on these parameters. However, such approaches are not suitable for causal inference as the outcomes are used in the posterior sampling of hyper-parameters. As a result, the design stage and the analysis stage are mixed, rendering the final estimates of causal effects biased (Rubin et al., 2008). In Section 3.2, we propose to use a GP-induced covariate balance metric for the selection of hyper-parameters, which only uses the observed exposure and covariates (w_i, c_i) .

3.1 Covariance function k for causal inference

The covariance function $k(\cdot, \cdot)$ (i.e. the kernel) of a GP is usually chosen to be stationary and to depend on the *distance* between two units in the covariate space. Different distance metrics imply different kernel functions. For example, the L_2 norm as a distance metric leads to a radial-basis function kernel and Matérn kernel. We propose a distance metric that relies on both the estimated GPS and exposures (Imbens, 2000; Wu et al., 2018). More specifically, we denote by $\hat{s}(w, c)$ the estimated GPS and we define k as

$$k((w, c), (w', c')) = \gamma^2 h \left(\frac{(\hat{s}(w, c) - \hat{s}(w', c'))^2}{\alpha} + \frac{(w - w')^2}{\beta} \right), \quad (3)$$

where $h : [0, \infty) \rightarrow [0, 1]$ is a non-decreasing function. Here α and β are scaling factors for estimated GPS and exposure levels respectively. We introduce α and β to control the relative importance of $\hat{s}(w, c)$ and w when determining the similarity of units. $\gamma > 0$ controls the overall scale of the GP. Our ultimate goal is to estimate $Y_i(w)$ using the GP model in (1) and to borrow information more heavily from units j 's that are as similar as possible to the unit i with exposure level w in terms of the kernel k defined above in (3).

We now show that with this specification of k , the estimator $\hat{R}(w)$ indeed identifies the actual CERF $R(w)$. To see this, we start by illustrating a connection between model (1) and an exact matching algorithm based on GPS. Assume $h(z) = \exp(-z)$ and $\mu(\cdot) = 0$. We show that the GP model (1) is equivalent to an exact matching algorithm on $(w, \hat{s}(w, c))$. The exact matching algorithm estimates $Y_i(w)$ with the observed outcome $\tilde{Y}_i(w) = y_j$ such that $\hat{s}(w, c_j) = \hat{s}(w, c_i)$ and $w_j = w$. The existence of subject j is hard to guarantee, especially when p is large. For simplicity, we assume that it exists for every i and w . The proof is in Supplementary Materials.

Proposition 1. *Under the model (1) with covariance function (3), if we assume $\mu = \sigma = 0$ and the prior for α and β as $\alpha \sim N(0, \sigma_1^2), \beta \sim N(0, \sigma_2^2)$, then the estimated $\hat{Y}_i(w)$ converges to $\tilde{Y}_i(w)$ when $\sigma_1^2 \rightarrow 0$ and $\sigma_2^2 \rightarrow 0$.*

When exact matching can be achieved, based on the property of GPS being a balancing function (Imbens, 2000) and the unconfoundedness assumption 1, the estimator $\hat{R}(w)$ is an unbiased estimator of the actual CERF $R(w)$ at any w , provided that the GPS model is correctly specified. In reality, exact matching is usually not feasible and instead of seeking the single observation with exactly the same w and $\hat{s}(w, c_i)$ to estimate $Y_i(w)$, we can focus on the observations in a neighborhood of $(w, \hat{s}(w, c_i))$. If the neighborhood is small enough, we can almost recover covariate balance, i.e., the distribution of the covariates are identical across neighborhoods centered around different $(w, \hat{s}(w, c))$. For example, in the original Medicare dataset, we find the correlation between $\text{PM}_{2.5}$ and NO_2 is large (> 0.4). However, if we consider two neighborhood sets $\mathcal{N}_1 = \{i : |w_i - 5| \leq 0.1, |\hat{s}(5, c_1) - \hat{s}(w_i, c_i)| \leq 0.01\}$ and $\mathcal{N}_2 = \{i : |w_i - 10| \leq 0.1, |\hat{s}(10, c_2) - \hat{s}(w_i, c_i)| \leq 0.01\}$, the absolute correlation between NO_2 and $\text{PM}_{2.5}$ for samples in $\mathcal{N}_1 \cup \mathcal{N}_2$ reduces to 0.03, indicating the

variable NO₂ has been rebalanced by limiting to only neighborhoods of $(w, s(w, c))$.

The following is the rationale that the posterior estimate $\hat{R}(w)$ from the GP has causal interpretation. The covariance function in GP defines a natural neighborhood around each $(w, \hat{s}(w, c_i))$ by virtue of the fact that posterior mean $\hat{Y}_i(w)$ is a weighted sum of a small set of y_k with $(w_k, \hat{s}(w_k, c_k))$ close enough to $(w, s(w, c_i))$. Therefore, $\hat{R}(w)$ is indeed derived based on observations from the union of covariate balanced neighborhood sets, which should preserve the balance to a high degree. Covariate balance can be estimated based on the weighting scheme induce by the GP model. The following proposition (see Supplementary Materials for the proof) illustrates the posterior consistency of $\hat{R}(w)$ when the GPS is known.

Proposition 2. *Let $\mu = 0$, $\alpha > 0$, $\beta > 0$ and $\gamma > 0$ be fixed. Assume that $\hat{s}(w, c)$ is the true conditional density of W given C . If Assumptions 1-3 hold, and in addition $E(Y|W = w, \hat{s}(w, C) = s)$ is continuously differentiable, then $\forall \epsilon > 0$*

$$\lim_{N \rightarrow \infty} \Pi \left(|\hat{R}(w) - R(w)| > \epsilon | \mathcal{S} \right) = 0, \text{ a.e. } P_0,$$

for any $w \in \mathcal{W}$. Here Π indicates the posterior probability and P_0 is the joint distribution of $\{Y_i, W_i, C_i\}_{i=1}^\infty$.

3.2 Weighting scheme of GP model and covariate balancing

Recall that under model (1), $\hat{Y}_i(w) = \mu(w, c_i) + \boldsymbol{\kappa}_i^\top(w) (\mathbf{K}_N + \sigma^2 I_N)^{-1} (\mathbf{y} - \mathbf{m})$. Let $\mathbf{a}_i(w) = (a_{i,j}(w); j = 1, \dots, N)^\top = (\mathbf{K}_N + \sigma^2 I_N)^{-1} \boldsymbol{\kappa}_i(w)$. Note that $\mathbf{a}_i(w)$ depends on γ and σ through the ratio γ/σ . We argue that $\mathbf{a}_i(w)$ defines a weighting scheme of all observed subjects for the estimation of $Y_i(w)$. To see this, we fix $\mu \equiv 0$ and it follows that $\hat{Y}_i(w) = \mathbf{a}_i(w)^\top \mathbf{y}$. When $k(\cdot, \cdot)$ is stationary, $\sum_j a_{i,j}(w) \approx 1$ and any $a_{i,j}(w)$ that is not negligible is positive, if w and c_i are not in the tails of the empirical distributions of W and C (Rasmussen, 2006). This result implies that $\hat{Y}_i(w)$ is (approximately) a weighted average of all the observed outcomes \mathbf{y} .

Since $\hat{R}(w) = N^{-1} \sum_i \hat{Y}_i(w)$, $\hat{R}(w)$ is also a weighted average of all the observed outcomes in \mathbf{y} and the weight for y_i is $a_{\cdot,i}(w) = N^{-1} \sum_{j=1}^N a_{j,i}(w)$. The collection of $a_{\cdot,i}(w)$ can be used to

define a covariate balance metric $\rho_r(w)$ for $r = 1, \dots, p$, which measures the weighted correlation between the r -th covariate and the continuous exposure W . We standardize the vector of observed exposure levels $\mathbf{w} = (w_1, \dots, w_N)$ and the covariate vector of subject i $\mathbf{c}_i = (c_{i,1}, \dots, c_{i,p})^\top$ by $\mathbf{w}^* = \sigma_w^{-1}(\mathbf{w} - \bar{w})$, where $\bar{w} = \sum_i a_{\cdot,i}(w)w_i$ and $\sigma_w = \sqrt{\sum_i a_{\cdot,i}(w)(w_i - \bar{w})^2}$, and $\mathbf{c}_i^* = \Sigma_c^{-1/2}(\mathbf{c}_i - \bar{\mathbf{c}})$, where $\bar{\mathbf{c}} = \sum_i a_{\cdot,i}(w)\mathbf{c}_i$ and $\Sigma_c = \sum_i a_{\cdot,i}(w)(\mathbf{c}_i - \bar{\mathbf{c}})(\mathbf{c}_i - \bar{\mathbf{c}})^\top$. The estimate of the weighted correlation between the r -th covariate and exposure W is $\hat{\rho}_r(w) = \sum_i a_{\cdot,i} w_i^* c_{i,r}^*$.

For casual inference, we would like to achieve low absolute correlation between w and every covariate, which can be assessed with $\hat{\rho}(w) = p^{-1} \sum_{r=1}^p |\hat{\rho}_r(w)|$. When estimating the population average CERF at a fixed set of M exposure levels $\{w_1, w_2, \dots, w_M\}$, the overall covariate balance score is $\hat{\rho} = M^{-1} \sum_{m=1}^M \hat{\rho}(w_m)$.

The metric $\hat{\rho}$ implies a tuning approach of hyper-parameters using only covariates and exposure but not observed outcome. We select α, β , and γ/σ by minimizing the overall covariate balancing score $\hat{\rho}$:

$$\hat{\alpha}, \hat{\beta}, \left(\frac{\hat{\gamma}}{\hat{\sigma}}\right) = \arg \min_{\alpha, \beta, \gamma/\sigma} \hat{\rho}(\alpha, \beta, \gamma/\sigma).$$

In practice, $\mathbf{a}_i(w)$ contains a lot of weights with negligible values and we will set them to be zero exactly (e.g. threshold = 10^{-5}). Additionally, if w or c_i is far from their observed population averages, $\sum_j a_{i,j}(w)$ will be smaller than 1 by a significant margin. In this case, we will re-normalize $\mathbf{a}_i(w)$ by $\sum_j a_{i,j}(w)$ after the initial truncation of negligible values.

The estimation of σ has to rely on the observed outcomes \mathbf{y} as σ captures the uncertainty of the outcomes directly. We propose to use the sample variance of the leave-one-out residuals to estimate σ^2 . Let $\hat{Y}(w_i, c_i)$ be the estimated outcome for sample i using $y_1, \dots, y_{i-1}, y_{i+1}, \dots, y_N$ and $e_i = y_i - \hat{Y}(w_i, c_i)$ the residual. We estimate σ^2 by $\hat{\sigma}^2 = \sum_i e_i^2 / (N - 1)$.

3.3 Nearest-neighbor GP for scalability

A main limitation of a GP model is its lack of scalability to datasets with large amount of observations due to the excessive computational cost of inversion of covariance matrices between observed outcomes. In our data application, there are 520,711 observations in the unstratified dataset and

a standard GP model such as that in (1) will be computationally intractable. We overcome this limitation by imposing a sparsity constraint on the covariance matrix between $Y(w, c)$ via a nearest-neighbor approach (Datta et al., 2016).

To review the idea of the nearest-neighbor GP (nnGP), we consider the joint distribution of \mathbf{Y} . It can be decomposed into a series of conditional distributions: $p(\mathbf{Y}) = p(Y_1) \cdot p(Y_2|Y_1) \cdot p(Y_N|Y_1, \dots, Y_{N-1})$. (1) implies that $Y_i|Y_1, \dots, Y_{i-1} \sim N(\tilde{m}_i, \tilde{\sigma}_i^2)$, where

$$\begin{aligned}\tilde{m}_i &= \mu(w_i, c_i) + \boldsymbol{\kappa}_{i,i-1}^\top (\mathbf{K}_{i-1} + \sigma^2 I_{i-1})^{-1} (\mathbf{y}_{i-1} - \mathbf{m}_{i-1}), \\ \tilde{\sigma}_{i-1}^2 &= k((w_i, c_i), (w_i, c_i)) + \sigma^2 - \boldsymbol{\kappa}_{i,i-1}^\top (\mathbf{K}_{i-1} + \sigma^2 I_{i-1})^{-1} \boldsymbol{\kappa}_{i,i-1},\end{aligned}$$

where $\mathbf{K}_i = (k((w_j, c_j), (w_k, c_k))); j, k = 1, \dots, i$, $\boldsymbol{\kappa}_{i,i'} = (k((w_i, c_i), (w_j, c_j))); j = 1, \dots, i'$, $\mathbf{y}_i = (y_1, \dots, y_i)^\top$ and $\mathbf{m}_i = (\mu(w_1, c_1), \dots, \mu(w_i, c_i))$.

Note that the expressions for \tilde{m}_i and $\tilde{\sigma}_i^2$ involve the matrix inversion $(\mathbf{K}_{i-1} + \sigma^2 I_{i-1})^{-1}$, which is computationally demanding when $i \leq N$ is large. nnGP reduces the computational cost for the estimation of \tilde{m}_i and $\tilde{\sigma}_i^2$ through a conditional independence assumption. Specifically, denote the top- ℓ nearest neighbors of subject i as $\mathcal{N}_{\ell,i}$, where the distances are determined by the coordinates $(w_i, \hat{s}(w_i, c_i))$, the nnGP assumes that $p(Y_i|Y_1, \dots, Y_{i-1}) = p(Y_i|\mathcal{N}_{\ell,i})$, which is equivalent to assume that Y_i and $\{Y_1, \dots, Y_{i-1}\} \setminus \mathcal{N}_{\ell,i}$ are independent conditioned on $\mathcal{N}_{\ell,i}$. As a result, the joint distribution of \mathbf{Y} can be expressed as a product of multiple low dimensional density functions $p(Y_i|\mathcal{N}_{\ell,i})$ and posterior inference based on this likelihood function will be much more scalable than a standard GP as N increases. Similarly, for any unobserved point $Y(w, c)$, the nnGP assumes that the conditional distribution $Y(w, c)|\mathbf{Y}$ only depends on the top- ℓ nearest neighbors of $(w, \hat{s}(w, c))$ in the observed N samples.

To understand the amount of computational complexity reduced by the nnGP, note that the conditional independence assumption introduced by nnGP makes the precision matrix of any collection of $Y(w, c)$ to be sparse. The inversion of such precision matrix comes with a computational complexity of $O(N\ell^3)$, which is much smaller than the complexity ($> O(N^2)$) associated with computing a precision matrix induced by a standard GP. A typical specification of an nnGP model is

described based on an associated standard GP model and requires an additional parameter ℓ , which indicates the size of the nearest-neighbor sets $\mathcal{N}_{\ell,i}$.

3.4 Estimating derivatives of ERC

We can estimate the derivatives of $Y_i(w)$ with respect to w provided $\mu(\cdot)$ and $k(\cdot, \cdot)$ is once differentiable with respect to w . Note that Gaussian kernel satisfies this requirement. Specifically, we are interested in estimating $\partial Y_i / \partial w = \lim_{\delta w \rightarrow 0} (Y(w + \delta w, c_i) - Y(w, c_i)) / \delta w$.

Based on the properties of a GP, $(\partial Y(w, c) / \partial w, Y(w', c'))$ also follows a GP with mean function $(\partial \mu(w, c) / \partial w, \mu(w', c'))$ and covariance function as

$$\begin{aligned} \text{cov}(Y(w, c), Y(w', c')) &= k((w, c), (w', c')), \\ \text{cov}\left(Y(w, c), \frac{\partial Y(w', c')}{\partial w'}\right) &= \frac{k((w, c), (w', c'))}{\partial w'}, \\ \text{cov}\left(\frac{\partial Y(w, c)}{\partial w}, \frac{\partial Y(w', c')}{\partial w'}\right) &= \frac{\partial^2 k((w, c), (w', c'))}{\partial w \partial w'}. \end{aligned} \tag{4}$$

Once all the hyper-parameters are selected, we can estimate the derivatives of $R(w)$ by noting that

$$\widehat{\frac{\partial R}{\partial w}} = \frac{1}{N} \sum_{i=1}^N \widehat{\frac{\partial Y(w, c_i)}{\partial w}},$$

where $\widehat{\frac{\partial Y(w, c_i)}{\partial w}}$ is the estimate of $\partial Y(w, c_i) / \partial w$. It can be the posterior mean of the GP in (4) conditioned on the observed data \mathbf{y} . If $\mu(\cdot)$, $k(\cdot, \cdot)$ and $\hat{s}(w, c)$ have higher order derivatives with respect to w , we can repeatedly apply (4) to estimate the higher order derivatives of $R(w)$ with respect to w .

4 Simulation Studies

We use simulation studies to examine the performance of our approach and compare it with four other approaches in the literature, including GPS adjustment estimator (Hirano and Imbens, 2004), inverse probability of treatment weighting (IPTW) estimator (Robins et al., 2000), and the non-

parametric doubly robust (DR) estimator (Bang and Robins, 2005; Kennedy et al., 2017), under different model specifications. We also include in our comparison the GPS matching algorithm (Wu et al., 2018). To estimate GPS, we first use gradient boosting algorithm (Chen and Guestrin, 2016) to approximate $E(W|C = c)$ and calculate $p(W|C)$ using a normal density with mean $E(W|C = c)$ and variance equal to the residual variance of the gradient boosting fit.

4.1 Simulation settings

We follow the specification in Wu et al. (2018) and assume that $C_i \in \mathbb{R}^6$ with five continuous components and one categorical component:

$$(C_{i,1}, \dots, C_{i,4}) \sim N(0, I_4), \quad C_{i,5} \sim \text{Categorical}\{-2, -1, 0, 1, 2\}, \quad C_{i,6} \sim U(-3, 3).$$

We generate W_i with the following six GPS models:

1. $W_i = 9[-0.8 + (0.1, 0.1, -0.1, 0.2, 0.1, 0.1)C_i] + 17 + N(0, 5)$
2. $W_i = 15[-0.8 + (0.1, 0.1, -0.1, 0.2, 0.1, 0.1)C_i] + 22 + T(2)$
3. $W_i = 9[-0.8 + (0.1, 0.1, -0.1, 0.2, 0.1, 0.1)C_i] + 1.5c_{i,3}^2 + 15 + N(0, 5)$
4. $W_i = \frac{49 \exp[-0.8 + (0.1, 0.1, -0.1, 0.2, 0.1, 0.1)C_i]}{1 + \exp[-0.8 + (0.1, 0.1, -0.1, 0.2, 0.1, 0.1)C_i]} - 6 + N(0, 5)$
5. $W_i = 42(1 + \exp[-0.8 + (0.1, 0.1, -0.1, 0.2, 0.1, 0.1)C_i])^{-1} - 18 + N(0, 5)$
6. $W_i = 7 \log[-0.8 + (0.1, 0.1, -0.1, 0.2, 0.1, 0.1)C_i] + 13 + N(0, 4)$

We generate y_i from an outcome model $[Y_i|W = w_i, C = c_i] \sim N(\mu_i, 10)$, where

$$\mu_i = -10 - (2, 2, 3, -1, 2, 2)c_i - w_i(0.1 - 0.1c_{i,1} + 0.1c_{i,4} + 0.1c_{i,5} + 0.1c_{i,3}^2) + 0.13^2 w_i^3$$

We will consider three different sample sizes, $N = 200, 1000, 5000$. We set the number of neighbors to be 25 for nnGP. For both GP implementations, we use the parameter tuning approach introduced in Section 3.2.

We evaluate the estimated $\hat{R}(w)$ based on two metrics, absolute bias and mean-squared error (MSE) to the true CERF $R(w)$. Assume we have S simulation replicates, the two metrics are defined as follows.

$$|\text{Bias}| = M^{-1} \sum_{m=1}^M \left| \sum_{s=1}^S \hat{R}_s(w_m) / S - R(w_m) \right|,$$

$$\text{MSE} = (MS)^{-1} \sum_{m=1}^M \sum_{s=1}^S (\hat{R}_s(w_m) - R(w_m))^2,$$

where w_1, \dots, w_M are equally spaced points from 0 to 20 and \hat{R}_s is the estimate of CERF in the s -th simulation. Note that all six specifications of W_i have the majority of the probability mass in $(0, 20)$. We report the $|\text{Bias}|$ and MSE for each approach across 50 simulate cycles where each cycle contains 50 simulation replicates. Finally, we will examine covariate balance imposed by the GP models by visualizing $\hat{\rho}$ across the simulation replicates.

4.2 Simulation results

We summarize the results of the simulations in Figure 2. We find that the absolute bias of the full GP model and GPS matching algorithm are very similar to each other across all six scenarios. nnGP on the other hand, has elevated variance of the estimates of \hat{R} , as indicated by the MSE but the sparsity approximation does not inflate the absolute bias of the Bayesian approach too much.

If the relationship between W and C is linear and the GPS values are not heavy-tailed (Scenario 1), all approaches have reasonable performance. The doubly robust approach reduces the bias and MSE compared to GPS adjustment approach and IPTW. When the relationship between W and C stays linear but GPS values are heavy-tailed and include extreme values (Scenario 2), GPS adjustment, IPTW and doubly robust estimators all produce very large MSE, and are not able to reduce confounding bias even with large samples. In contrast, matching based approaches, including our GP model and the GPS matching algorithm, are all robust to the extreme GPS values, creating much more stable estimation than the other three estimators. Although the absolute bias and MSE are much larger than in Scenario 1 and the rates of decrease for the absolute bias and MSE are

smaller, matching-based algorithms are able to leverage the incremental information and are not negatively affected by extreme GPS values.

When $E(W|C)$ is non-linear, as depicted in Scenario 3-6, all approaches tend to have higher MSE and absolute bias compared to the first two scenarios. However, since the error terms are all normally distributed, the extreme behavior of GPS adjustment and doubly robust estimators observed in Scenario 2 is not replicated. The estimated GPS from gradient boosting has the smallest accuracy when the actual $E(W|C)$ is a log function (Scenario 6), in which GPS adjustment has significantly higher bias and MSE than all other approaches. GP models and GPS matching algorithms have the lowest bias among all estimators except for Scenario 6, where doubly robust estimator has the lowest bias, while their efficiency is uniformly smaller than doubly robust estimator across all four scenarios. Sample size seems to have relatively low impact on the bias, indicating the misspecification of GPS is the main contributor of the observed bias.

We also examine the covariate balance induced by the GP models. In Supplementary Figure 1, we illustrate the distribution of the optimized $\hat{\rho}$ across simulation replicates for all six scenarios, three sample sizes and two GP models (full GP and nnGP). We can see except for the case where GPS is heavy-tailed (Scenario 2) and sample size is small ($N = 200$), the covariate balance scores are well below 0.1. $\hat{\rho}$ as well as its variability across replicates decrease as sample size increases. At moderate sample size $N = 1000$, $\hat{\rho}$ in Scenario 2 can also be maintained below 0.1.

4.3 Detecting change-point with derivatives

In this section, we use simulated data to examine the ability of our GP model to detect change points of the CERF. We simulate data under the assumption that the true CERF is continuous and piece-wise linear. The place where two linear pieces connect is a change point. Specifically, we

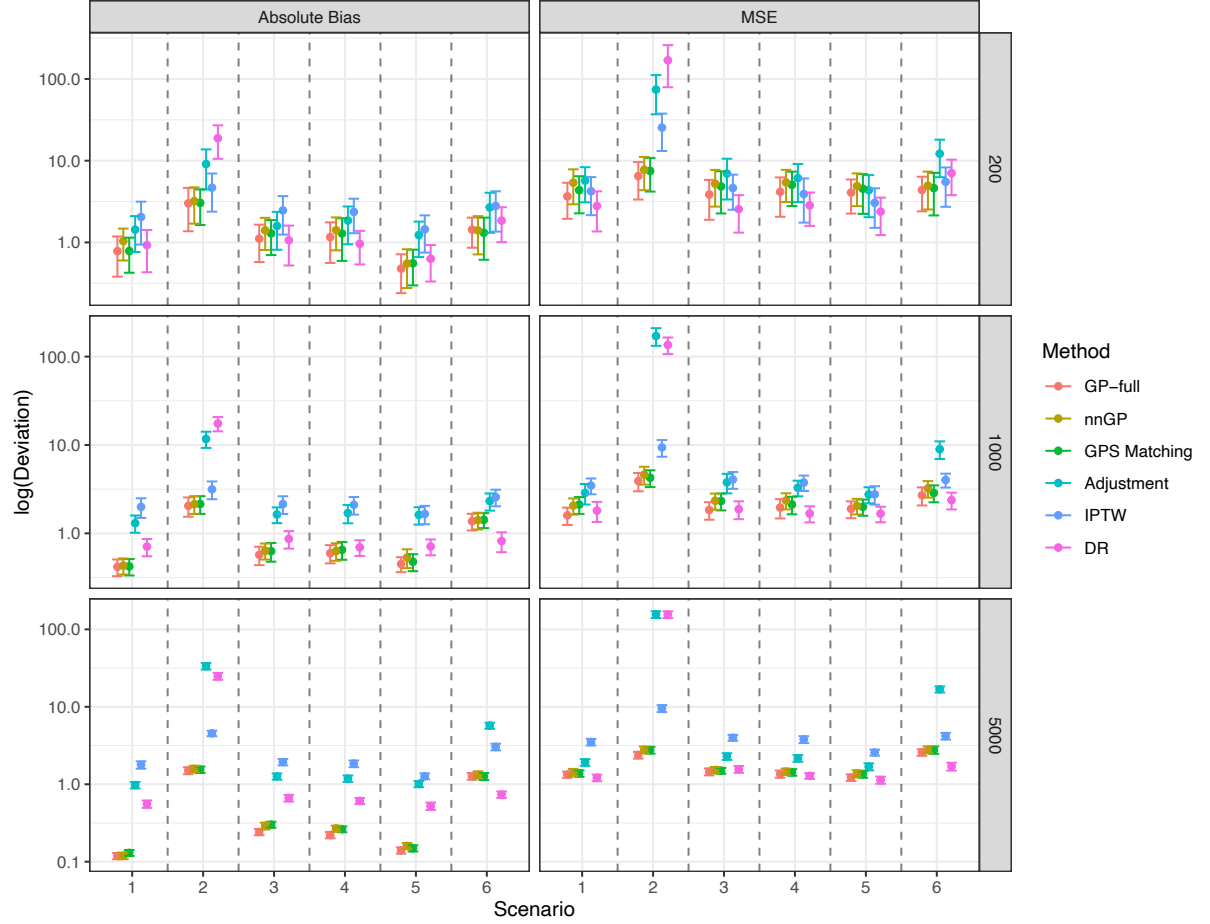


Figure 2: Comparisons of different CERF estimation methods across simulations. We evaluate the accuracy of the estimates by two metrics, absolute bias and mean squared error (MSE). The error bars indicate one standard deviation of the metric over 50 simulation cycles, in which 50 replicates are performed. Scenarios are as defined in Section 4.1. GP-full: the complete GP model; nnGP: nearest-neighbor approximated GP with neighbor size 25; GPS matching: caliper matching in Wu et al. (2018); Adjustment: including GPS as a covariate in the outcome model; IPTW: inverse probability of treatment weighting estimator; DR: doubly-robust estimator in Kennedy et al. (2017).

assume that

$$\begin{aligned}\mu_i = & -10 - (2, 2, 3, -1, 2, 2)c_i - w_i(0.1 - 0.1c_{i,1} + 0.1c_{i,4} + 0.1c_{i,5} + 0.1c_{i,3}^2) \\ & + \mathbb{I}(2.5 < w_i < 5)(10w - 25) + 25\mathbb{I}(5 \leq w < 10) + \mathbb{I}(10 \leq w_i < 12.5)(10w - 75) \\ & + \mathbb{I}(12.5 \leq w_i < 17.5)(2.5(w_i - 12.5) + 50) + 62.5\mathbb{I}(17.5 \leq w < 20).\end{aligned}$$

We simulate c_i as in Section 3.1 and we use the first GPS model in Section 3.1.

In Figure 3, we illustrate the estimated $R(w)$ and its first derivative $\partial R(w)/\partial w$ using full GP and nnGP (50 neighbors) respectively. We find that both approaches recover the true CERF accurately while the estimates from nnGP tend to have larger uncertainty. The estimated first derivative is indeed a smoothed version of the actual derivative (solid lines in bottom panels). However, we find that places where the credible intervals of $\partial \hat{R}(w)/\partial w$ first become completely above or below zero have high correspondence with the actual change points, which provide an empirical approach for change point detection.

5 Analysis of Medicare dataset with GP

We first apply the proposed GP model on the age-sex adjusted mortality rate $\hat{\lambda}_{i,t}$ (520,711 observations) and then on each of the four stratum (see Table 1 for numbers of observations) separately to estimate the overall and stratum-specific causal effects of $\text{PM}_{2.5}$ on all-cause mortality. We use the log-transformed mortality rate as the outcome and the covariates for ZIP-code i and year t are denoted as $c_{i,t}$. $c_{i,t}$ contains all 18 ZIP-code-level covariates, ozone and NO_2 concentrations as well as year. Denote the measurement of $\text{PM}_{2.5}$ at ZIP-code i and year t as $w_{i,t}^{(p)}$. Note that $w_{i,t}^{(p)}$ and $c_{i,t}$ remain the same across all strata. We assume that $(\hat{\lambda}_{i,t,g}, w_{i,t}^{(p)}, c_{i,t})$ are independent for all i and t within a stratum. For the remainder of this section, we will replace subscript i in Section 3 with (i, t) or (i, t, g) to emphasize that the unit observation in this dataset is indexed jointly by ZIP-code, year and stratum.

For the overall CERF estimation based on $\log(\hat{\lambda}_{i,t})$, we estimate GPS for $\text{PM}_{2.5}$ using all 520,711

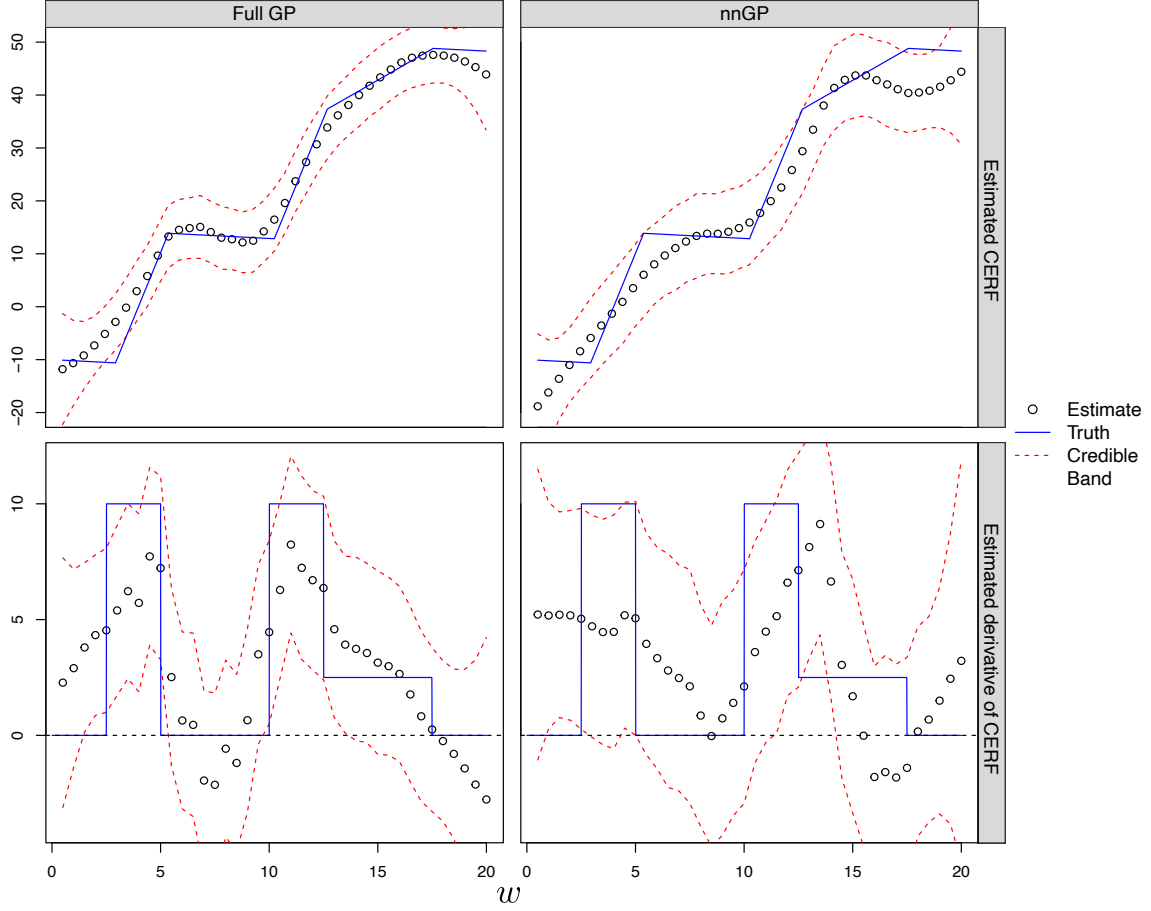


Figure 3: *Detecting change points by estimates of derivatives in simulations. We use a piece-wise linear function to introduce the change points (blue lines). Left two panels are results based on a full GP model whereas the right panels correspond to an nnGP fit on the same data.*

ZIP-code-by-year observations. For the stratified CERFs, we estimate stratum-specific GPS instead. We assume that the conditional distribution of $w^{(p)}$ given C is a normal distribution. We estimate the conditional mean of this distribution with a gradient boosting machine (Chen and Guestrin, 2016) and the conditional variance is approximated by the residual variance. We tune the hyper-parameters separately for each stratum and the aggregated dataset. We calculate the covariate balance score $\hat{\rho}$ with $M = 100$ equidistant levels throughout the exposure range $2\text{-}18 \mu\text{g}/\text{m}^3$, which are roughly the 0.5 and 99.5 percentile of the observed $\text{PM}_{2.5}$ levels. We use a Gaussian kernel in this application and implement the nnGP approximation to the standard GP model. We set the number of nearest neighbors to be 200.

Based on the selected hyper-parameters, we estimate the CERF of $\text{PM}_{2.5}$ on all-cause mortality. We exponentiate the posterior means derived from the GP models to recover the estimated all-cause mortality rate $\hat{R}(w)$. We recover the entire CERF $R(w)$ with the estimates $\hat{R}(w)$ on 100 equidistant levels of the exposure and calculate the derivative of $\hat{R}(w)$ with respect to w based on (4). The statistical uncertainty associated with these estimates are derived using the posterior distribution of the related parameters.

In Figure 4, we visualize the results for the unstratified data. In the left panel, we illustrate the estimated CERF $\hat{R}(w)$ at different levels of $\text{PM}_{2.5}$. We observe that the adjusted mortality rate increases as $\text{PM}_{2.5}$ increases. The rate of increase is large when $\text{PM}_{2.5}$ is lower than $5\mu\text{g}/\text{m}^3$ and higher than $15\mu\text{g}/\text{m}^3$ and relatively small when $\text{PM}_{2.5}$ is between $7.5\mu\text{g}/\text{m}^3$ and $12.5\mu\text{g}/\text{m}^3$. From the middle panel of Figure 4, we can find the rate of increase is only significantly different from zero when $\text{PM}_{2.5} \leq 10\mu\text{g}/\text{m}^3$, indicating a change point of the effect of $\text{PM}_{2.5}$ on all-cause mortality at around $10\mu\text{g}/\text{m}^3$. In the right panel, we illustrate the correlations between $\text{PM}_{2.5}$ and all other variables in the original data and when each observation is weighted according to the tuned GP. We find that the GP model indeed improves covariate balance.

In Figure 5 top panels, we illustrate the estimated stratum-specific CERFs of $\text{PM}_{2.5}$. We note that younger strata (< 75 year) have much lower mortality rate than the older strata. Female tends to have slightly lower mortality rate than male. Elevated $\text{PM}_{2.5}$ levels lead to increase in mortality rate when $\text{PM}_{2.5} \leq 5\mu\text{g}/\text{m}^3$. When the level of $\text{PM}_{2.5}$ is medium to high ($> 10 \mu\text{g}/\text{m}^3$), an

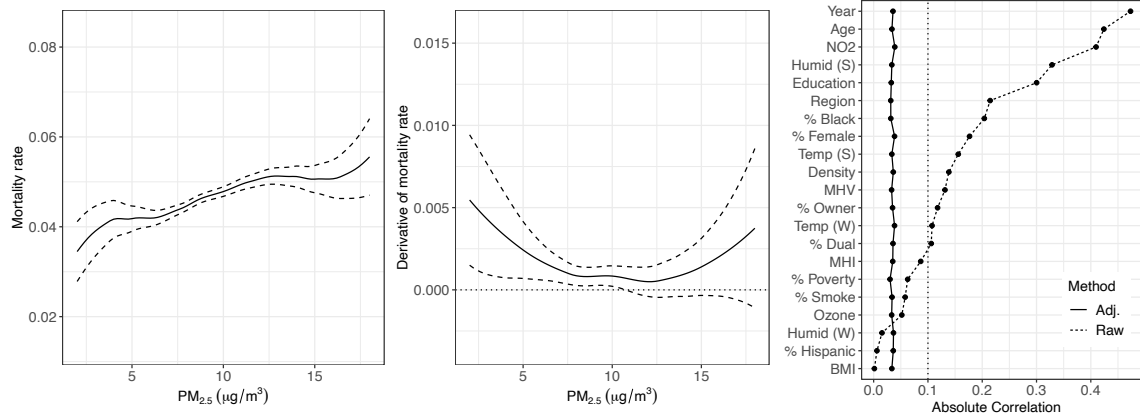


Figure 4: Results of the unstratified analysis based on the age-sex adjusted mortality rate $\hat{\lambda}_{i,t}$. **(Left)** Estimated CERF for $PM_{2.5}$ on the all-cause mortality rate. **(Middle)** Estimated derivatives of CERF with respect to the exposure level of $PM_{2.5}$. Dashed lines indicate point-wise 95% posterior credible bands for the two estimated curves. **(Right)** Raw and GP-induced (Adj.) absolute correlations between $PM_{2.5}$ and all other variables. We assume that all ZIP-code-by-year observations are independent. The GP is tuned using the unstratified data. Age = average age at enrollment; Education = proportion of below high school education; Humid (S) and (W) = average summer and winter humidity; Region = census region; Temp (S) and (W) = average summer and winter temperature; Density = population density; % Owner = % owner-occupied housing; % Dual = proportion of dual eligibility of Medicare and Medicaid; MHV = median home value; MHI = median household income; BMI = average BMI.

increase in $\text{PM}_{2.5}$ only leads to minimum changes in the mortality rate. In Supplementary Figure 2 top panels, we normalize $\hat{R}(w)$ by its value at $w = 2\mu\text{g}/\text{m}^3$. The results indicate that age and sex are no longer effect modifiers of $\text{PM}_{2.5}$ in terms of fold-changes in mortality rate. Again, a significant increase in mortality rate is observed at low $\text{PM}_{2.5}$ level.

We then estimate the derivative of mortality rate with respect to the exposure level to identify potential change points for the effect of $\text{PM}_{2.5}$. In Figure 5 bottom panels, we illustrate the estimated derivatives for $\text{PM}_{2.5}$ in each strata. It is clear that for all strata except for the older male strata, a change point at around $5 - 10\mu\text{g}/\text{m}^3$ is present, below which one unit increase in $\text{PM}_{2.5}$ level leads to significant increase in mortality rate. This is consistent with published results Wei et al. (2020), in which the change of death probability associated with one unit increase in long-term exposure to $\text{PM}_{2.5}$ reaches its maximum at $10\mu\text{g}/\text{m}^3$. The rates of changes are larger in the older strata than in the younger strata. The derivatives of mortality rate ratio $\hat{R}(w)/\hat{R}(2)$ with respect to levels of $\text{PM}_{2.5}$ have similar behaviors as exposure to $\text{PM}_{2.5}$ increases. But no significant difference is present across strata (see Supplementary Figure 2 bottom panels).

Finally, we illustrate in Figure 6 the raw and GP-induced absolute correlations of $\text{PM}_{2.5}$ to other covariates in different strata. We calculate these correlations using all observations in a stratum, and the GP-induced correlations are calculated using observation-specific weights imposed by the tuned GPs. Compared to the raw correlations, we can see GP-induced correlations are all below 0.1.

6 Discussion

We proposed a Bayesian nonparametric model based on GP for the estimation of causal effects of continuous exposures. This model leverages the GPS learned from a flexible machine learning algorithm to adjust for the observed potential confounders. In addition, the posterior inference of the model parameters provides a natural characterization of the uncertainty of these causal estimates. We introduced a covariate balance score for the selection of hyper-parameters in the GP model to overcome the mixing of design and analysis stages caused by traditional parameter tuning

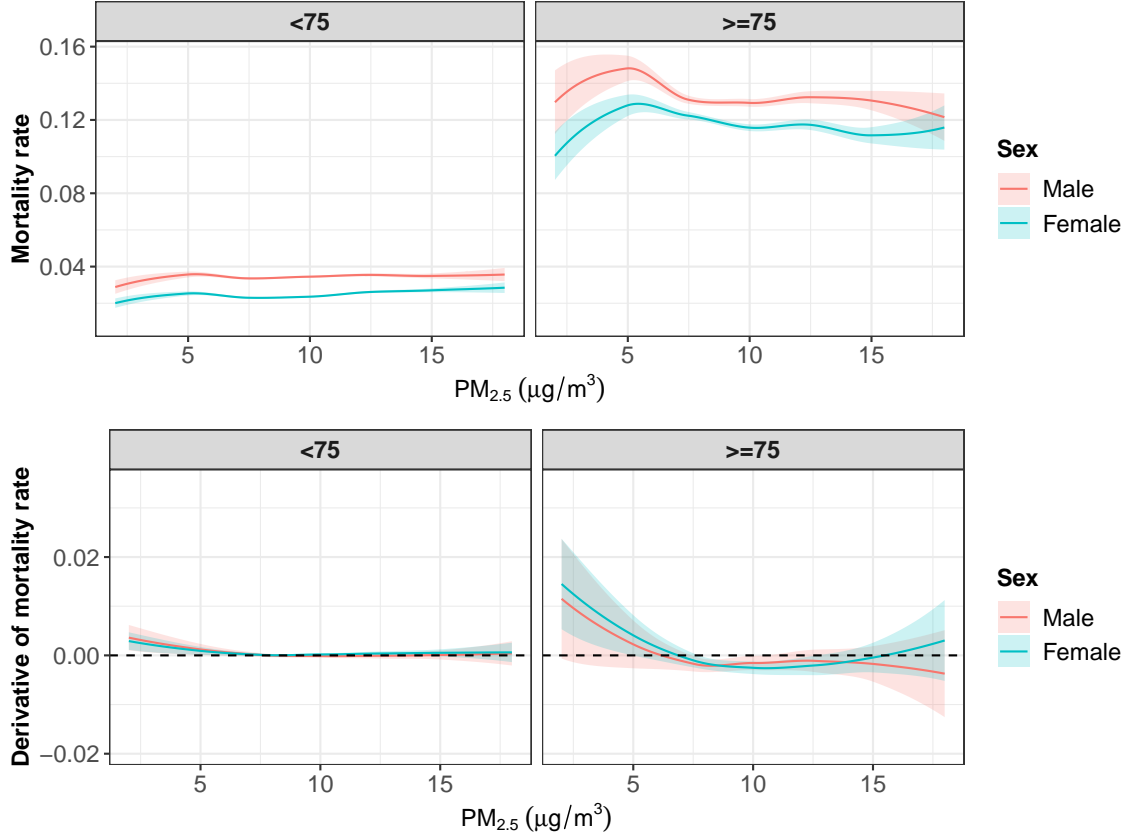


Figure 5: (**Top**) Estimated mortality rate as a function of exposure level of $PM_{2.5}$ for all four strata. The shaded area indicates 95% posterior credible bands. For all strata we observe an increase in mortality rate when the level of long-term exposure to $PM_{2.5}$ increases. The younger/female strata (< 75 year) have lower mortality rate than the older/male strata. (**Bottom**) Derivative of mortality rate with respect to exposure levels of $PM_{2.5}$. Shaded areas indicate 95% posterior credible bands. The Y-axis is $\partial \hat{R}(w)/\partial w$. In all strata except for the older male stratum, a change point at $5 - 10 \mu g/m^3$ is observed at which the credible bands of the derivatives cover zero and the derivatives are no longer significantly different from zero. The rate of increase in mortality rate is larger in older strata than in younger strata.

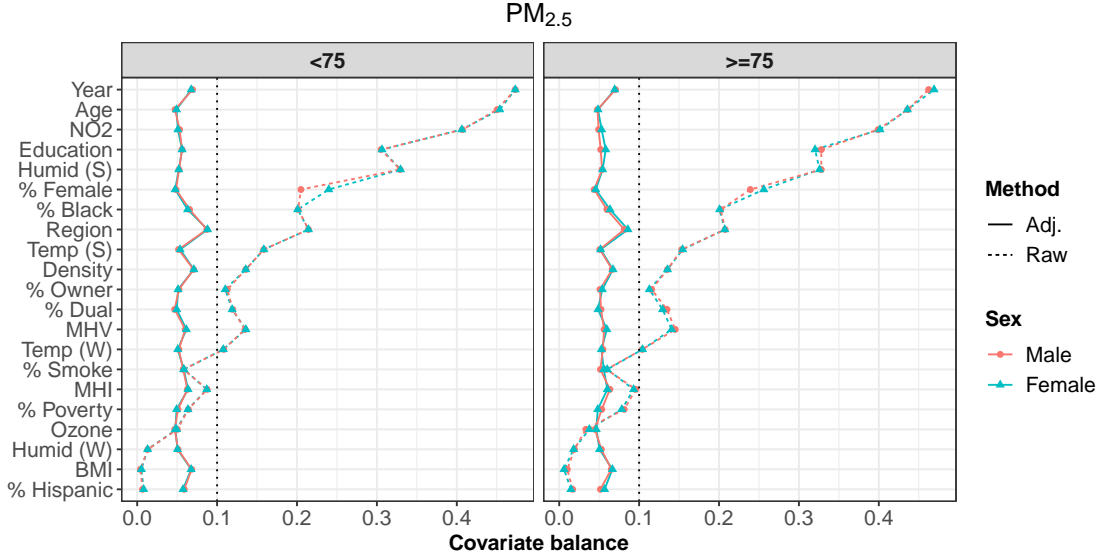


Figure 6: Absolute correlations of $PM_{2.5}$ to all other covariates when observations are weighted according to the GPs (Adj.) and not weighted (Raw). We visualize the correlations for all four strata separately. Every correlation is based on all observations (i, t, g) in stratum g with $\hat{\lambda}_{i,t,g}$ available. We calculate the weighted correlation for covariate r using $M^{-1} \sum_w \hat{\rho}_r(w)$ and the unweighted correlations are Pearson correlations. We assume that all observations in a stratum are independent. The GPs are tuned in each stratum separately. Age = average age at enrollment; Education = proportion of below high school education; Humid (S) and (W) = average summer and winter humidity; Region = census region; Temp (S) and (W) = average summer and winter temperature; Density = population density; % Owner = % owner-occupied housing; % Dual = proportion of dual eligibility of Medicare and Medicaid; MHV = median home value; MHI = median household income; BMI = average BMI.

approaches of GP models. We proved that this Bayesian model is equivalent to an exact matching scheme based on GPS and observed exposure levels and further illustrate that the estimated causal effect derived from our model is consistent, provided the GPS is correctly identified and no unmeasured confounders are present. The closed-form expression of derivatives of a GP enables us to characterize the rate of changes of the causal effects when the exposure level changes and in turn provides a heuristic approach to detect change points on the CERF. A simulation study shows that our model has comparable performance to a recently proposed GPS matching algorithm for the estimation of CERFs (Wu et al., 2018) with slight increase in MSE. The simulation study also verifies that the heuristic approach of change point detection is effective. An application of our model for the estimation of the effect of $\text{PM}_{2.5}$ on all-cause mortality illustrates that the Bayesian model is scalable when coupled with an nnGP approximation and that our results are consistent with previous findings.

From a methodological perspective, this model can serve as a foundation for a Bayesian framework that can resolve various issues in the estimation of causal effects of continuous exposures. For example, we can incorporate a model for $p(W, C)$ to take into account measurement errors in covariates. From an application perspective, the results on $\text{PM}_{2.5}$ reveal potential change points at which a phase transition in the causal effects is observed. It also has relevant policy-making implications: reducing $\text{PM}_{2.5}$ further is necessary as the increase of mortality rate associated with increases in $\text{PM}_{2.5}$ is most significant when $\text{PM}_{2.5}$ is in the low to mid level.

Throughout the application section, we make the strong assumption that all ZIP-code-by-year observations are independent. We account for the spatiotemporal variation in observations by including year and census region in the GPS model. This assumption can be relaxed by augmenting the two-dimensional index of the GP with time and geographic locations. The other major limitation that is worth investigating further is the estimation of GPS. Currently, we use a separate machine learning method to construct the GPS model and use the estimated GPS for (w, c_i) as if it has no statistical uncertainty. As a result, the final characterization of the uncertainty in $\hat{R}(w)$ is too optimistic. A unified model for $p(Y(w)|C)$ and $p(W|C)$ can be employed to resolve this issue, where a flexible model for $p(W|C)$ can be introduced to mitigate the potential misspecification of the GPS.

Bayesian models, for instance those introduced in Giffin et al. (2020) are suitable candidates for this unified approach.

Finally, we want to point out that in the data application we use directly the estimated mortality rate as the outcome and ignore the uncertainty associated with the estimation. As a result, the posterior credible bands are often too optimistic. We would like to extend the GP model in this paper by incorporating a link function and a distribution family of the outcome to directly analyze count data or other types of data that cannot be depicted by a normal distribution. We will focus on the computational aspect of this extended model as the posterior inference would require some form of approximation, likely through variational inference.

7 Acknowledgement

The authors are grateful to Rachel Nethery for helpful discussions. Funding was provided by the Health Effects Institute (HEI) grant 4953-RFA14-3/16-4, National Institute of Health (NIH) grants R01 GM111339, R01 ES024332, R01 ES026217, R01 ES028033, R01 MD012769, R01 AG066670, R01 MH120400, R33 DA042847, DP2 MD012722 and Gunderson Legacy Fund grant 041622.

References

- Bang, H. and Robins, J. M. (2005). Doubly robust estimation in missing data and causal inference models. *Biometrics*, 61(4):962–973.
- Berhane, K. and Molitor, N.-T. (2008). A bayesian approach to functional-based multilevel modeling of longitudinal data: applications to environmental epidemiology. *Biostatistics*, 9(4):686–699.
- Chartered Clean Air Scientific Advisory Committee (2018). Summary Minutes of the U.S. EPA CASAC Public Teleconference on Particulate Matter.
- Chen, T. and Guestrin, C. (2016). Xgboost: A scalable tree boosting system. In *Proceedings of the 22nd acm sigkdd international conference on knowledge discovery and data mining*, pages 785–794.

- Colangelo, K. and Lee, Y.-Y. (2020). Double debiased machine learning nonparametric inference with continuous treatments. *arXiv preprint arXiv:2004.03036*.
- Datta, A., Banerjee, S., Finley, A. O., and Gelfand, A. E. (2016). Hierarchical nearest-neighbor gaussian process models for large geostatistical datasets. *Journal of the American Statistical Association*, 111(514):800–812.
- Di, Q., Amini, H., Shi, L., Kloog, I., Silvern, R., Kelly, J., Sabath, M. B., Choirat, C., Koutrakis, P., Lyapustin, A., et al. (2019a). Assessing no₂ concentration and model uncertainty with high spatiotemporal resolution across the contiguous united states using ensemble model averaging. *Environmental science & technology*, 54(3):1372–1384.
- Di, Q., Amini, H., Shi, L., Kloog, I., Silvern, R., Kelly, J., Sabath, M. B., Choirat, C., Koutrakis, P., Lyapustin, A., et al. (2019b). An ensemble-based model of pm_{2.5} concentration across the contiguous united states with high spatiotemporal resolution. *Environment international*, 130:104909.
- Di, Q., Dai, L., Wang, Y., Zanobetti, A., Choirat, C., Schwartz, J. D., and Dominici, F. (2017a). Association of short-term exposure to air pollution with mortality in older adults. *Jama*, 318(24):2446–2456.
- Di, Q., Wang, Y., Zanobetti, A., Wang, Y., Koutrakis, P., Choirat, C., Dominici, F., and Schwartz, J. D. (2017b). Air pollution and mortality in the medicare population. *New England Journal of Medicine*, 376(26):2513–2522.
- Dominici, F. and Zigler, C. (2017). Best practices for gauging evidence of causality in air pollution epidemiology. *American Journal of Epidemiology*, 186(12):1303–1309.
- EPA (2019). *Integrated Science Assessment (ISA) for Particulate Matter*.
- Giffin, A., Reich, B., Yang, S., and Rappold, A. (2020). Generalized propensity score approach to causal inference with spatial interference. *arXiv preprint arXiv:2007.00106*.

- Goldman, G. T. and Dominici, F. (2019). Don’t abandon evidence and process on air pollution policy. *Science*, 363(6434):1398–1400.
- Hernán, M. Á., Brumback, B., and Robins, J. M. (2000). Marginal structural models to estimate the causal effect of zidovudine on the survival of hiv-positive men. *Epidemiology*, pages 561–570.
- Hill, A. B. (1965). The environment and disease: association or causation?
- Hirano, K. and Imbens, G. W. (2004). The propensity score with continuous treatments. *Applied Bayesian modeling and causal inference from incomplete-data perspectives*, 226164:73–84.
- Imbens, G. W. (2000). The role of the propensity score in estimating dose-response functions. *Biometrika*, 87(3):706–710.
- Kallus, N. and Santacatterina, M. (2019). Kernel optimal orthogonality weighting: A balancing approach to estimating effects of continuous treatments. *arXiv preprint arXiv:1910.11972*.
- Kennedy, E. H., Ma, Z., McHugh, M. D., and Small, D. S. (2017). Nonparametric methods for doubly robust estimation of continuous treatment effects. *Journal of the Royal Statistical Society. Series B, Statistical Methodology*, 79(4):1229.
- Pope III, C. A., Cropper, M., Coggins, J., and Cohen, A. (2015). Health benefits of air pollution abatement policy: Role of the shape of the concentration–response function. *Journal of the Air & Waste Management Association*, 65(5):516–522.
- Rasmussen, C. E. (2006). Gaussian processes for machine learning. MIT Press.
- Requia, W. J., Di, Q., Silvern, R., Kelly, J. T., Koutrakis, P., Mickley, L. J., Sulprizio, M. P., Amini, H., Shi, L., and Schwartz, J. (2020). An ensemble learning approach for estimating high spatiotemporal resolution of ground-level ozone in the contiguous united states. *Environmental Science & Technology*, 54(18):11037–11047.
- Robins, J. M. (2000). Marginal structural models versus structural nested models as tools for causal inference. In *Statistical models in epidemiology, the environment, and clinical trials*, pages 95–133. Springer.

- Robins, J. M., Hernán, M. Á., and Brumback, B. (2000). Marginal Structural Models and Causal Inference in Epidemiology. *Epidemiology*, 11(5).
- Robins, J. M., Rotnitzky, A., and Zhao, L. P. (1994). Estimation of regression coefficients when some regressors are not always observed. *Journal of the American statistical Association*, 89(427):846–866.
- Rosenbaum, P. R. and Rubin, D. B. (1983). The central role of the propensity score in observational studies for causal effects. *Biometrika*, 70(1):41–55.
- Rubin, D. B. et al. (2008). For objective causal inference, design trumps analysis. *Annals of Applied Statistics*, 2(3):808–840.
- Rubin, D. B. and Thomas, N. (1996). Matching using estimated propensity scores: relating theory to practice. *Biometrics*, pages 249–264.
- Schulz, J. and Moodie, E. E. (2020). Doubly robust estimation of optimal dosing strategies. *Journal of the American Statistical Association*, pages 1–13.
- Van der Laan, M. J. and Rose, S. (2011). *Targeted learning: causal inference for observational and experimental data*. Springer Science & Business Media.
- Vegetabile, B. G., Griffin, B. A., Coffman, D. L., Cefalu, M., Robbins, M. W., and McCaffrey, D. F. (2021). Nonparametric estimation of population average dose-response curves using entropy balancing weights for continuous exposures. *Health Services and Outcomes Research Methodology*, 21(1):69–110.
- Wang, Y. and Zubizarreta, J. R. (2019). Minimal dispersion approximately balancing weights: asymptotic properties and practical considerations. *Biometrika*, 107(1):93–105.
- Wei, Y., Wang, Y., Wu, X., Di, Q., Shi, L., Koutrakis, P., Zanobetti, A., Dominici, F., and Schwartz, J. D. (2020). Causal effects of air pollution on mortality rate in massachusetts. *American journal of epidemiology*, 189(11):1316–1323.

- Wu, X., Braun, D., Schwartz, J., Kioumourtzoglou, M., and Dominici, F. (2020). Evaluating the impact of long-term exposure to fine particulate matter on mortality among the elderly. *Science advances*, 6(29):eaba5692.
- Wu, X., Mealli, F., Kioumourtzoglou, M.-A., Dominici, F., and Braun, D. (2018). Matching on generalized propensity scores with continuous exposures. *arXiv preprint arXiv:1812.06575*.
- Zubizarreta, J. R. (2012). Using mixed integer programming for matching in an observational study of kidney failure after surgery. *Journal of the American Statistical Association*, 107(500):1360–1371.
- Zubizarreta, J. R. (2015). Stable weights that balance covariates for estimation with incomplete outcome data. *Journal of the American Statistical Association*, 110(511):910–922.
- Zubizarreta, J. R., Paredes, R. D., Rosenbaum, P. R., et al. (2014). Matching for balance, pairing for heterogeneity in an observational study of the effectiveness of for-profit and not-for-profit high schools in chile. *The Annals of Applied Statistics*, 8(1):204–231.